Depositional sequence characterization based on seismic variational mode decomposition

Fangyu Li[1], Bo Zhang[2], Rui Zhai[1], Huailai Zhou[3], and Kurt J. Marfurt[1]

Abstract

Subtle variations in otherwise similar seismic data can be highlighted in specific spectral components. Our goal is to highlight repetitive sequence boundaries to help define the depositional environment, which in turn provides an interpretation framework. Variational mode decomposition (VMD) is a novel data-driven signal decomposition method that provides several useful features compared with the commonly used time-frequency analysis. Rather than using predefined spectral bands, the VMD method adaptively decomposes a signal into an ensemble of band-limited intrinsic mode functions, each with its own center frequency. Because it is data adaptive, modes can vary rapidly between neighboring traces. We address this shortcoming of previous work by constructing a laterally consistent VMD method that preserves lateral continuity, facilitating the extraction of subtle depositional patterns. We validate the accuracy of our method using a synthetic depositional cycle example, and then we apply it to identify seismic sequence stratigraphy boundaries for a survey acquired in the Dutch sector, North Sea.

Introduction

Seismic stratigraphy often forms one of the key components of seismic interpretation, and it requires the analysis of the reflection amplitude, continuity, reflection configuration, and external form (Mitchum et al., 1977; Cross and Lessenger, 1988). Seismic stratigraphy provides a means to identify sequence stratigraphy and sedimentary cycles. Patterns in the seismic data, including onlaps, offlaps, downlaps, truncations, and other features, allow a skilled interpreter to define whether a given sequence corresponds to transgressive, regressive, or other stages. Ligtenberg et al. (2006) use the Wheeler transform (or chronostratigraphic) based on the principle of superposition to define geologic events and lithologic units representing a relative geologic time scale. Such seismic stratigraphy, and hence sequence stratigraphy information, is buried in conventional seismic amplitude volumes (Hart, 2013), although the quality of seismic data itself limits the extraction of this information.

In the presence of coherent and random noise, sequence boundaries may be buried and thus overlooked on amplitude volumes. Fortunately, this noise may exhibit spectral responses different than those of the underlying signal, suggesting that one may be able to separate the two. Zeng (2013) finds the expression of sequence boundaries to be frequency dependent, in which their seismic expression appears quite different if different frequency bands are used. For this reason, spectral decomposition should be able to aid in distinguishing between transgressive and regressive facies in seismic data (Liu et al., 2015). And, we wish to evaluate data-driven signal decomposition as an alternative method to commonly used spectral decomposition methods.

The Fourier transform forms the basis of most spectral analysis tools, and it provides stationary (not time-variant) frequency information. Han and van der Baan (2013) report that because the seismic spectrum changes with time, the nonstationary data analyzed using the time-frequency analysis (TFA) method can be beneficial. The short-time Fourier transform (STFT) (Partyka et al., 1999; Lu and Li, 2013) and the continuous wavelet transform (CWT) (Sinha et al., 2005) are two popular TFA tools. These linear analysis methods are constrained by the Heisenberg uncertainty principle, which trades off increased temporal resolution with decreased spectral resolution, or increased spectral resolution with decreased temporal resolution (Tary et al., 2014). Matching pursuit (MP)-based TFA approaches achieve the highest vertical resolution, whereby the

waveforms that are drawn from a mother wavelet library are matched to a seismic trace in an iterative process favoring events with the highest spectral energy (Wang, 2007; Wang et al., 2016). The choice of wavelet library and fitting methods is critical for the performance of MP methods, which sometimes fail to match the lower energy events at the low/high frequencies.

Huang et al. (1998) propose the popular data-driven empirical-mode decomposition (EMD) signal decomposition method to analyze nonstationary signals (Kaplan et al., 2009; Han and van der Baan, 2013; Tary et al., 2014; Honorio et al., 2016). Because EMD decomposes the data into nonband-limited intrinsic mode functions (IMFs), it suffers from frequency mixture issues, making the meaning of the results more difficult to interpret. To address this drawback, Dragomiretskiy and Zosso (2014) develop the variational mode decomposition (VMD) to decompose a nonstationary signal into an ensemble of band-limited IMFs. Liu et al. (2016) compare VMD with the alternative of EMD-based methods, and they find that VMD can express the same seismic data with fewer intrinsic modes. The STFT, CWT, and MP spectral decompositions provide laterally consistent images for each spectral component. Unfortunately, because each trace is decomposed independently, the characteristics of the "first" or most important EMD or VMD component will vary laterally. Even though one can use these trace-by-trace algorithms to suppress noise components (K. J. Marfurt and F. Li, personal communication, 2017), vertical slices through any given VMD or EMD component provide little interpretational value. It is this lateral continuity that we wish to improve.

We begin our paper with a review of the basic theory of VMD. We then describe a laterally consistent VMD method designed to better delineate laterally continuous seismic stratigraphic patterns. We use a synthetic sedimentary model to validate VMD's capability in sedimentary pattern recognition. Finally, we apply VMD to a survey containing deltaic facies acquired in the Dutch sector, North Sea, and we conclude with an evaluation of adaptive signal decomposition in analyzing its seismic sequence stratigraphy.

Variational mode decomposition

Huang et al. (1998) propose EMD to decompose a data series into a finite set of IMFs. In EMD, the IMF, which represents different oscillations embedded in the data, is calculated in the time domain. To be an IMF, a signal must satisfy two criteria: (1) The number of local maxima and the number of local minima must differ by at most one, and (2) the mean of its upper and lower envelopes (a smooth curve outlining signal extremes) must equal zero. EMD has the form:

$$s(t) = \sum_{k=1}^{K} \text{IMF}_k(t) + r_K(t), \qquad (1)$$

where IMF_k is the kth IMF of the signal and r_K stands for the residual trend. The number K of EMD outputs

cannot be controlled. Liu et al. (2016) also find that very small unexpected oscillatory interference patterns can change the number of final output modes.

In contrast to EMD, VMD obtains IMFs that exhibit specific sparsity properties in the frequency domain. In VMD, the IMFs are defined as elementary amplitude/frequency modulated harmonics that can model the nonstationarity and the nonlinearity of the data (Appendix A). The frequency spectrum of every IMF is shifted to the baseband by mixing with an exponential function tuned to the respective estimated center frequency. The sparsity of every IMF is constrained by its bandwidth in the frequency domain with the IMF being relatively compact about an "oscillation" ω_k, which needs to be determined as part of the decomposition.

In VMD, the IMFs are extracted concurrently instead of recursively, which is achieved by solving the following optimization problem:

$$\min_{\{u_k, \omega_k\}} \left\{ \sum_k \left\| \partial_t \left[\left(\delta(t) + \frac{j}{\pi t} \right) * u_k(t) \right] e^{-j\omega_k t} \right\|_2^2 \right\}$$
$$\text{s.t.} \sum_k u_k = d(t), \qquad (2)$$

where u_k and ω_k are modes and their center frequencies, respectively, $\delta(\cdot)$ is a Dirac impulse, and $d(t)$ are the data to be decomposed. The term $(\delta(t) + j/\pi t)*u_k(t)$ is the Hilbert transform of u_k, which is defined in Appendix B. The constraint condition requires that the summation over all modes should approximate the input data.

Traditionally, VMD determines the IMFs trace by trace, such that lateral consistency across the survey may not be preserved. Because seismic data represent the depositional environment, preserving lateral continuity where it exists is critical. Honorio et al. (2016) apply the EMD-based methods trace by trace, and they observe gaps and "jumps" between neighboring traces. To address this problem, we add lateral consistency constraints in the optimization object function. VMD is achieved by solving the following problem:

$$\min_{\{u_k, \omega_k\}} \left\{ \sum_k \{ \| \nabla[u_{k,A}(\mathbf{t}) e^{-j\langle \boldsymbol{\omega_k}, \mathbf{t} \rangle}] \|_2^2 + \| P_s u_{k,A}(\mathbf{t}) \| \} \right\}$$
$$\text{s.t.} \sum_k u_k = d(t), \qquad (3)$$

where ∇ is the gradient operator; $u_k(\mathbf{t})$ are the 2D modes and their analytic formats $u_{k,A}(\mathbf{t})$ are described in equation B-3; $\boldsymbol{\omega_k}$ are the center frequency vectors; $d(\mathbf{t})$ is the signal to be decomposed, and in the seismic application, it is the vertical seismic section; and $\mathbf{P}_s$ is the 2D Wiener prediction filter based on $u_{k,A}(\mathbf{t})$. (Besides the constraint in equation 3, for the 3D application we adopt the mode center frequencies from the neighboring lines as the initial value of the current line, which strengthens the continuity between different lines).

Figure 1 displays a vertical seismic section with IMF-1, IMF-2, and IMF-3 computed using the traditional trace-by-trace VMD method. Note that the lateral consistency is lost. Even a small oscillation can totally change the decomposition results. Such instabilities are a common drawback of high-resolution decomposition methods, in which it is difficult to suppress noise and structural artifacts can appear. The IMF-2 and IMF-3 in Figure 1 have almost no interpretational value because of these artifi-cial discontinuities between neighboring traces. Figure 2 shows the IMFs from the laterally consistent VMD. The events in Figure 2c and 2d are continuous and reasonable. Note that the events in Figure 2b–2d can be combined to explain the reflection changes in Figure 2a, which can be helpful for seismic interpretation. Thus, the lateral consistency reinforcement is necessary and effective. In addition, Appendix C explains why it is valid to decompose seismic data into IMFs.
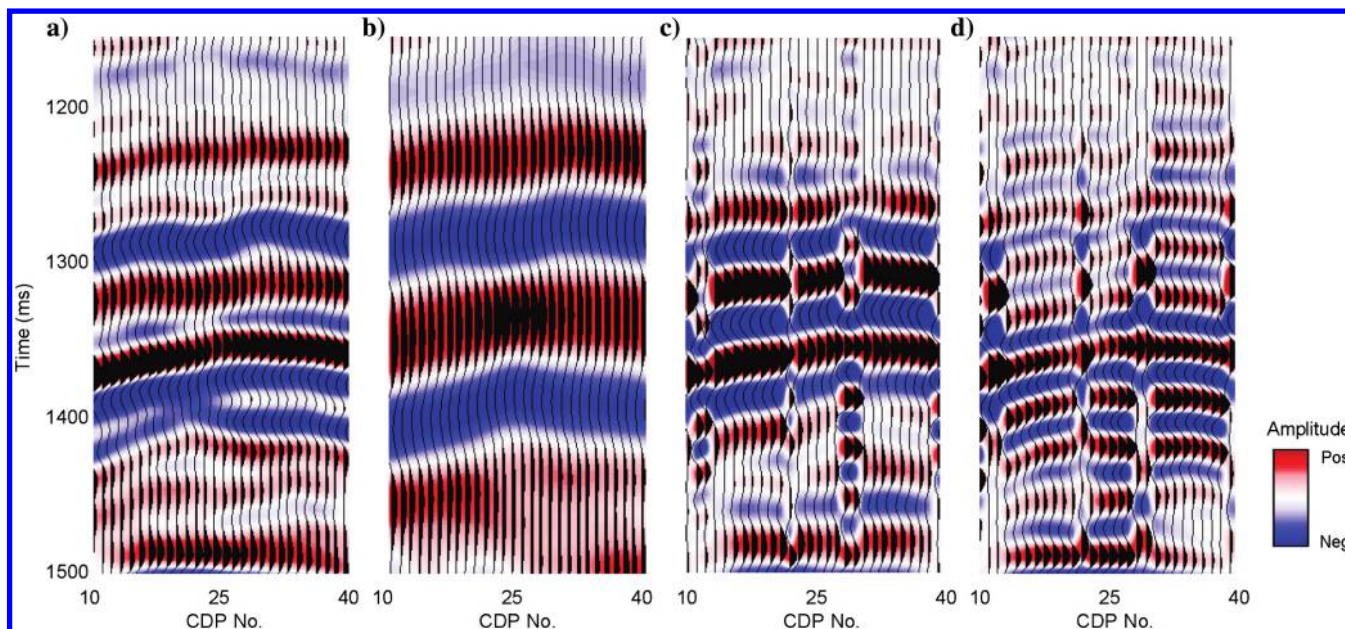

Figure 1. IMFs from traditional VMD. (a) Seismic and (b) IMF-1, (c) IMF-2, and (d) IMF-3. Note that the low-frequency mode section is continuous, but IMF-2 and IMF-3 show poor lateral consistency.
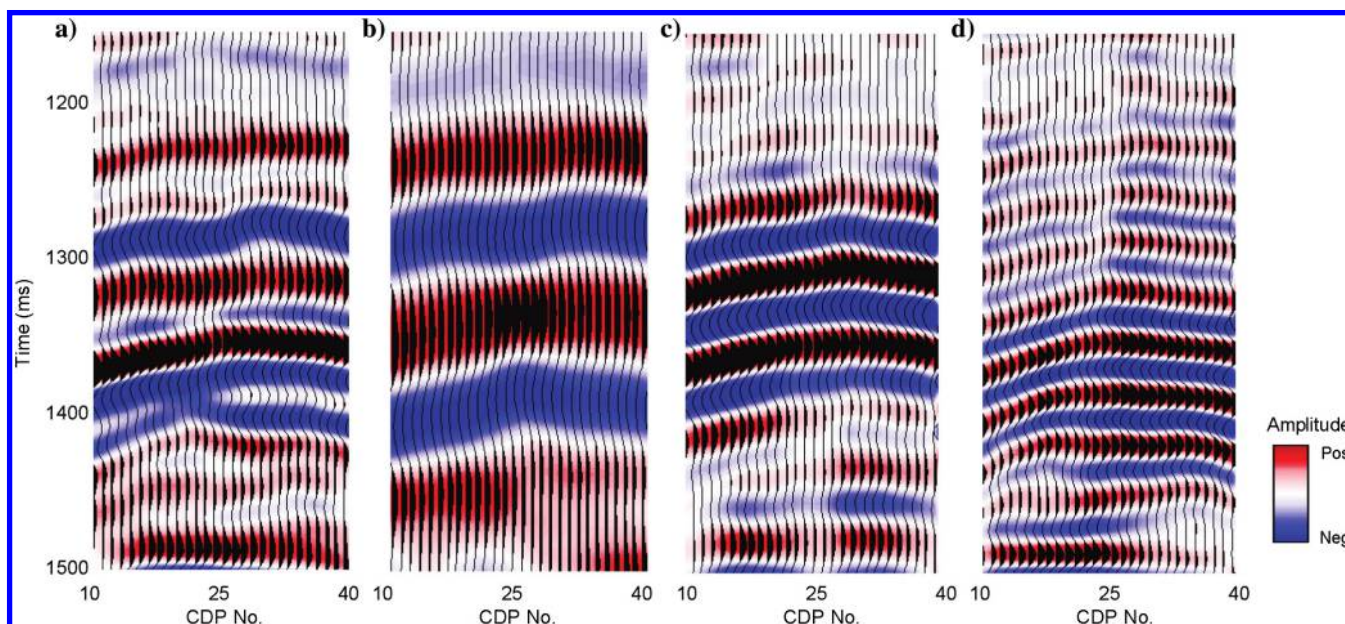

Figure 2. IMFs from laterally consistency constrained VMD. (a) Seismic and (b) IMF-1, (c) IMF-2, and (d) IMF-3 correspond with Figure 1b–1d, respectively. All the decomposed modes are continuous laterally because of the constraint in the VMD calculation equation.

Synthetic depositional sequence characterization

Besides seismic reflection analysis, sequence stratigraphy interpretation can be made based on rock composition, grain size characteristics, spontaneous potential, and gamma-ray log shapes (Rider, 1999). The transgressive/regressive facies recognition is the key for the stratigraphic sequence division. Well logging, which is usua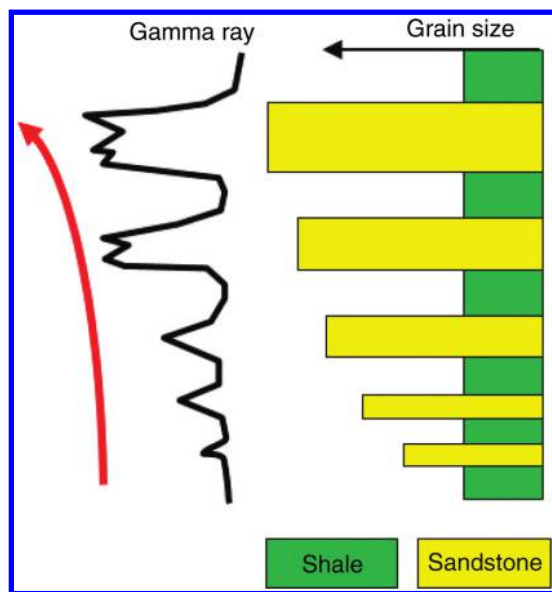lly the source of the geology information, is limited to discrete and widely spaced sampling points within a survey area. For this reason, we wish to determine the sedimentary and depositional environment for most areas of interest from the seismic data.

Following Rider (1999) and Martins-Neto and Catuneanu (2010), we build a single cycle of a delta progradational model. The percentage of sandstone increases upward, grain size changes from fine to coarse, with the sandstone interbedded with similar thick shale layers. Figure 3 shows that the gamma-ray log decreases upward, annotated by the depositional settings. Figure 4 shows the synthetic reflectivity series and the corresponding 60 m long seismic amplitude response. The reflectivity series follows the same pattern as the gamma ray in Figure 3. Because the grain size changes, the seismic reflectivity between shale and sandstone also changes with the depth. We apply VMD to the synthetic seismic data, and we obtain IMF-1, IMF-2, and IMF-3 (Figure 4). Note that the IMF-1 exhibits the same trend as the gamma-ray log in Figure 3, and IMF-2 and IMF-3 display other high-frequency information.

Figure 3. Gamma-ray log shape and depositional setting of deltaic progradational depositional trends, modified from Rider (1999). The sandstone is coarsening upward, and its thickness is also increasing upward interbedded with similar thick shale. The gamma-ray value becomes smaller upward.
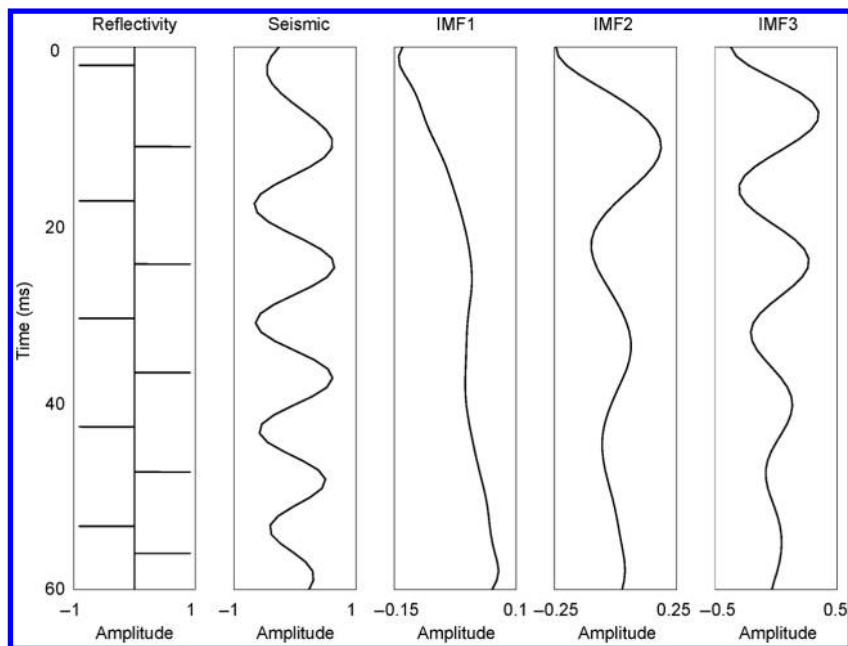
Field applications

The field data set used in the examples is from the southern North Sea Basin. After complex multiple stages of orogeny, rift, and subsidence that occurred during Paleozoic and Mesozoic times, the southern North Sea Basin experienced an inversion during the Tertiary. High sediment influx from neighboring highlands that uplifted in the late Miocene filled the basin, resulting in a prograding fluvio-deltaic system. This system (part of the giant Eridanos delta) constitutes the siliciclastic shelf deposits within the Pliocene interval with the thickness ranging from 350 to 430 m in the study area (Overeem et al., 2001). Several localized unconformities were formed during the deposition process (Ghazi, 1992; Sales, 1992; Gautier, 2003).

The 3D prestack time migration seismic data clearly image the large-scale sigmoidal stratal configuration. The dominant frequency is approximately 45 Hz, and the effective bandwidth is from 10 to 60 Hz in the study time window. Four wells are used in seismic-to-well calibration (Figure 5a). The deltaic cycles in the Dutch sector range from river-dominated to wave-tide-dominated stages. These cycles exhibit classic clinoform geometries prograding toward the basin (Patruno et al., 2015). Figure 5b shows our sequence stratigraphy interpretation. Based on the recognition of seismic reflection termination patterns (toplap, onlap, downlap, and truncation [Figure 5b]), five regional and local subaerial unconformities (SUs), two maximum regressive surfaces (MRSs), two maximum flooding surfaces (MFSs), and three basal

Figure 4. Reflectivity series, corresponding seismic trace, and IMF-1, IMF-2, and IMF-3 of the delta progradational model in Figure 3. Note that the amplitude of IMF-1 decreases upward like the gamma-ray log in Figure 3.

surfaces of forced regression (BFSRs) are defined using a seismic sequence stratigraphic interpretation workflow (Mitchum et al., 1977; Vail et al., 1977, 1987; Posamentier and Allen, 1999). According to the sequence boundaries, positions, and parasequence stacking patterns, the Pliocene strata of the study area can be divided into four third-order sequences (SQs). Furthermore, a complete depositional sequence is divided into four system tracts: (1) lowstand systems tract (LST), (2) transgressive systems tract (TST), (3) highstand systems tract (HST), and (4) falling stage systems tract (FSST) on the basis of the principles of quadripartite division for the sea-level cycle (Hunt and Tucker, 1992, 1995; Plint and Nummedal, 2000), such as SQ-1 and SQ-2 in Figure 5b. Because of the erosion when the relative sea level dropped, SQ-3 and SQ-4 form incomplete depositional records. The delta system that prograded across the continental shelf during the FSST stage deposited thick sandstone. In the base-level rising stage (TST and HST), nonuniform thickness mudstone draped over the delta sandstone.

The drawback of filter bank

The most common spectral component extraction method is to band-pass filter the seismic data. The vertical seismic section in Figure 5a shows deltaic facies. We extract a trace (denoted by a red triangle in Figure 5a) and display its spectrum in Figure 6, and we note that the main energy of the spectrum falls between 3 and 80 Hz. We design a suite of band-pass filters (0–27, 28–55, and 56–83 Hz) to separate the spectral components. Figure 7a demonstrates the band-pass filter design, and Figure 7b displays the filtered spectra of the different spectral bands (SBs), which have been normalized on every SB. Figure 8 shows the band-pass-filtered data. Similar expressions can be found on different SBs. As expected, the thicknesses of the seismic events change from large to small with the increasing frequency. Figure 8a displays the low-frequency component, which is relatively continuous. However, there are discontinuous artifacts between neighboring traces as shown in Figure 8b and 8c, which should be brought from the band-pass spectral decomposition. The filter bank breaks the seismic spectrum based on the predefined frequency ranges instead of the intrinsic modes of the data, resulting in discontinuities of waveforms.

The value of adaptive mode decomposition

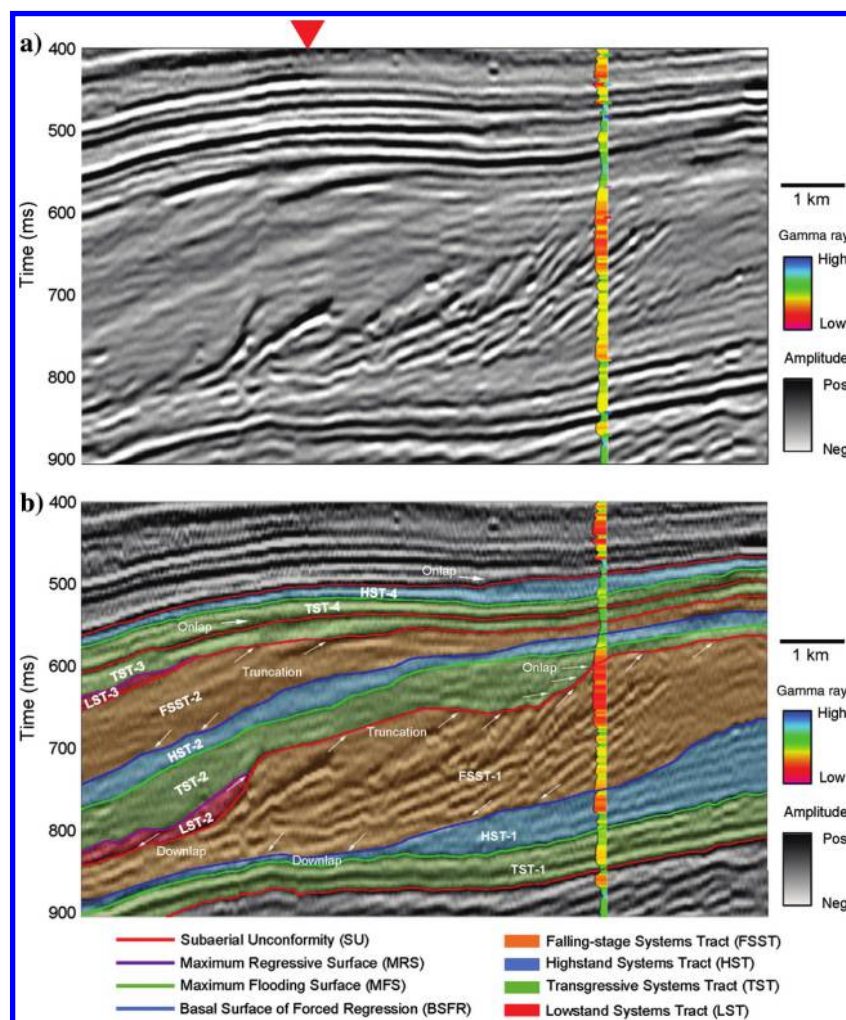To obtain the sequence stratigraphy interpretation in Figure 5b, we spend effort on sequence boundary iden-

Figure 5. A vertical well with posted gamma-ray log and a vertical slice through the seismic amplitude volume perpendicular to the shelf (a) without and (b) with sequence stratigraphy interpretation. According to the recognized isochronous stratigraphic interfaces, the Pliocene strata are divided into four third-order sequences (SQ). From the onset of base-level rise to the end of base-level fall, one complete base-level cycle is divided into four stages: LST, TST, HST, and FSST; SQ-1 and SQ-2 contain relative complete system tracts, and SQ-3 and SQ-4 only retain the strata records of base-level rising because of regional erosion.
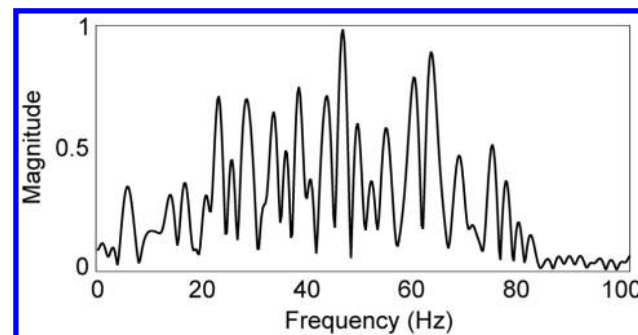

Figure 6. The normalized spectrum of the trace is denoted by a red triangle in Figure 5a.

tification, especially when the seismic reflections are not clear. As discussed above, signal decomposition methods can highlight specific components commonly buried in the seismic data. Because the filter bank method failed in assisting seismic stratigraphy interpretation, we applied VMD, a data-driven mode decomposition method, on the seismic data. Figure 9 shows the spectra of IMFs of the trace denoted by a red triangle in Figure 5a. Unlike the spectra in Figure 7b, every IMF is an ensemble spectral component, which is not strictly limited to a certain band. Figure 10a–10c displays the vertical sections of IMF-1, IMF-2, and IMF-3, respectively. The IMF-1 in Figure 10a shows the low-frequency background. Compared with Figure 8a, IMF-1 has a lower dominant frequency, but it also shows some details brought from the high frequencies. The IMFs from VMD are more continuous because there are no artificial discontinuities between neighboring traces. Compared with the results in Figures 8 and 10, the conflicts between human-defined methods and data-driven approaches are obvious. The parameter predefined decomposition arbitrarily divides seismic data into SBs, and this could result in the deformation of a geologic structure in waveform. Nonetheless, the adaptive decomposition we adopted can keep the relative completeness of intrinsic modes buried in the seismic signal, which reveals hidden geology information.

In Figure 10, stratigraphic terminations, such as onlap, toplap, downlap, and truncation, are labeled, as Figure 5b. In Figure 10a, the SUs, MFSs, and BSFR show strong energies. We can also observe the onlap, toplap, downlap, and truncation features. In Figure 10b, the onlaps, toplaps, and downlaps are very clear, as are the

stratal clinoforms, which are of low amplitude and hard to observe in Figure 5a. The SUs and MFSs show high amplitudes on IMF-3. Although the stratigraphy details are not clearly shown in Figure 10c, we can have a
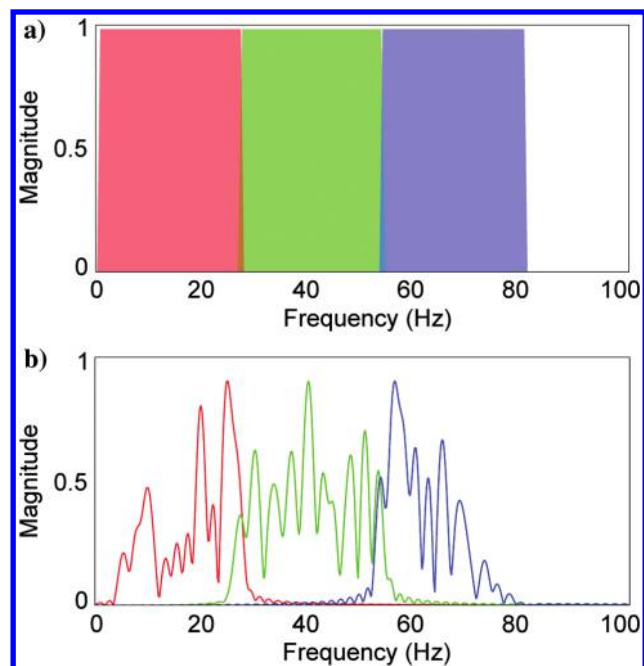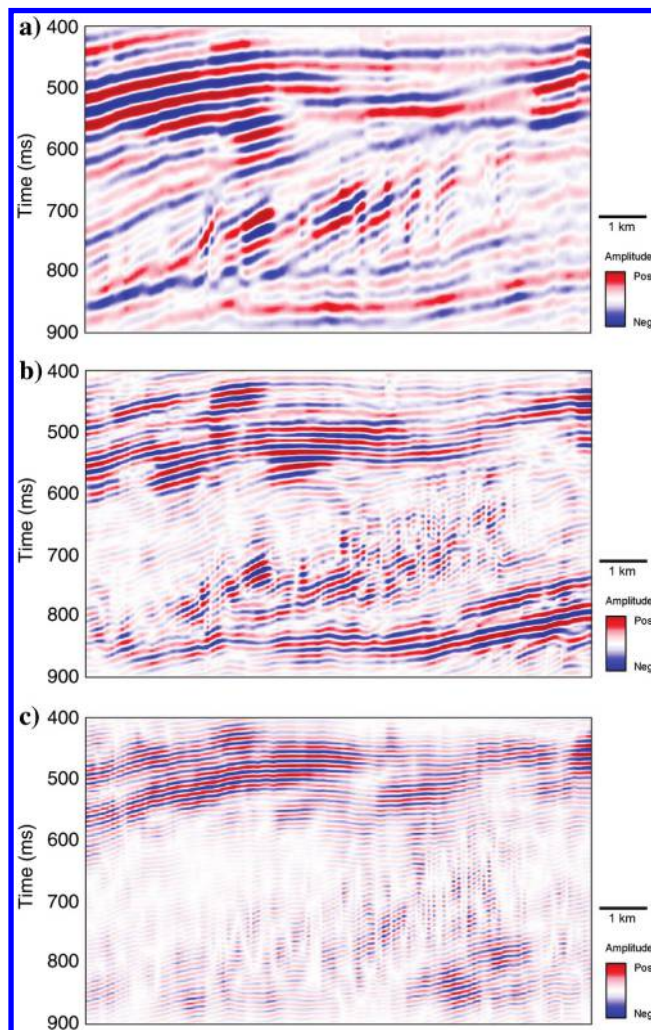

Figure 8. Band-pass filtered components: (a) 0–27, (b) 28–55, and (c) 56–83 Hz. The apparent vertical discontinuities in the resulting images are artifacts due to filtering and have little to do with the depositional environment or structural changes, making the analysis of such images difficult.
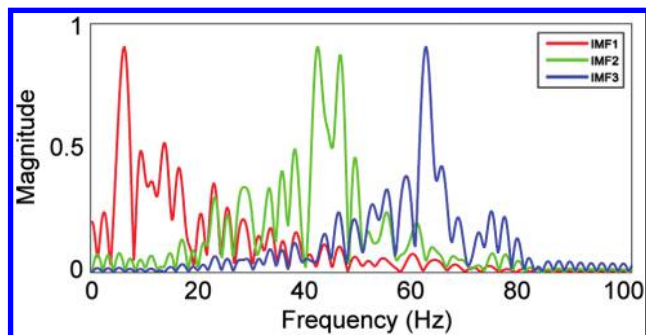

Figure 7. (a) Band-pass filter design with three SBs: 0–27, 28–55, and 56–83 Hz. (b) Filtered spectra with normalization on every SB.

Figure 9. The spectra of IMFs of the trace are denoted by a red triangle in Figure 5a with normalization of each mode.
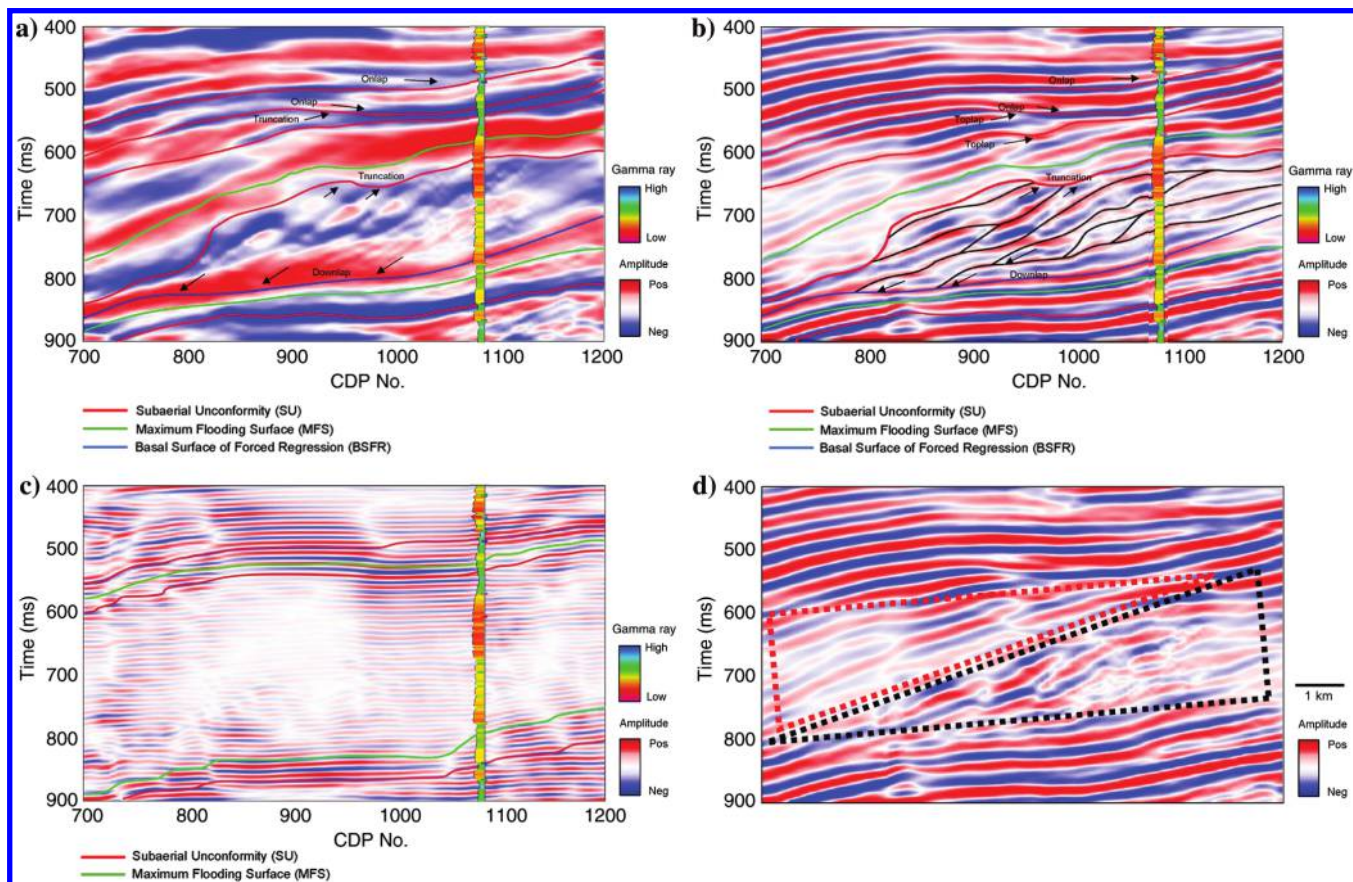
Figure 10. Sequence stratigraphy interpretation on (a) IMF-1, (b) IMF-2, and (c) IMF-3, corresponding to Figure 5b. Note the improved lateral continuity compared with the spectral decomposition image shown in Figure 8. The high amplitudes on IMF-1 highlight SUs, MFSs, and BSFR. Stratigraphy terminations are clear in IMF-1 and IMF-2, with the clinoform more clearly imaged by IMF-2. The SUs and MFSs exhibit high amplitudes on IMF-3, but the stratigraphy details seen in IMF-1 and IMF-2 are not clear. In general, the components needed to generate a sequence stratigraphic interpretation are more clearly imaged on IMFs than in the broadband input data shown in Figure 5a and band-pass filtered data in Figure 8. (d) By blending additional IMF-1 and IMF-2, one can delineate the two depositional SQs, SQ-1 and SQ-2 (shown as a dotted triangle).

rough conception of where the clinoform is. In Figure 10d, IMF-1 and IMF-2 are color blended together. Two depositional sequences, SQ-1 and SQ-2, show up more clearly, compared with the original seismic section. Thanks to the new details, the VMD does assist the stratigraphy interpretation.

Discussion

Machine-learning facies analysis tools usually project n attributes residing in an n-dimensional space onto a lower (in our case, 2D) dimensional deformed manifold. In general, there is little large-scale spatial information provided to the classification, because the IMFs provided by VMD provide such large-scale (specifically, sedimentary layering) patterns. Because of the improved lateral consistency, VMD IMF components form an excellent candidate as an input to machine-learning-based seismic facies classification (Zhao et al., 2017). We also hypothesize that by their addition, one can incorporate the seismic stratigraphy patterns that are effectively used by skilled interpreters into the classification result (Li et al., 2016b).

The choice of which IMF or collection of IMFs to use requires calibration with geologic control. Ideally, well logs provide the necessary ground truth.

Conclusions

Using the seismic data and a limited number of well logs, we evaluate the use of VMD in the identification of the depositional sequences. We find that laterally consistent VMD provides images amenable to detailed sequence stratigraphic interpretation, providing components that are easier to interpret than either the broadband input data or the more commonly used band-pass filtered (spectral voices) versions of the data.

Acknowledgments

Laboratory of Oil and Gas Reservoir Geology and Exploitation, Chengdu University of Technology (CDUT). We express our gratitude to the industry sponsors from the Attribute-Assisted Seismic Processing and Interpretation Consortium at the University of Oklahoma for their financial support. We would like to acknowledge dGB Earth Sciences for the donations of their software.

Appendix A

Intrinsic mode function

Intrinsic mode functions are amplitude-modulated-frequency-modulated signals that are written as

$$u_k(t) = A_k(t)\cos(\phi_k(t)), \qquad \text{(A-1)}$$

where the phase $\phi_k(t)$ is a nondecreasing function of $\phi_k'(t) \geq 0$, and the envelope is nonnegative $A_k(t) \geq 0$. The envelopes of $A_k(t)$ and the instantaneous frequency $\omega_k(t) = \phi_k'(t)$ vary and are slower than the phase $\phi_k(t)$ (Gilles, 2013). In other words, on a sufficiently long interval, the mode $u_k(t)$ can be considered as a pure harmonic signal.

Appendix B

Analytic signal

Let $s(t)$ be a real signal, then the complex analytic signal is defined as

$$s_A(t) = s(t) + i\mathscr{H}(s(t)) = s(t) * \left(\delta(t) + \frac{i}{\pi t}\right), \quad \text{(B-1)}$$

where $\mathscr{H}(\cdot)$ is the Hilbert transform and $*$ denotes the convolution operation.

The analytic signal of IMF in equation A-1 can be expressed as

$$u_{k,A}(t) = u_k(t) * \left(\delta(t) + \frac{i}{\pi t}\right). \qquad \text{(B-2)}$$

Following a definition in Bülow and Sommer (1999), we can define the 2D analytic signal of IMF as

$$u_{k,A}(\mathbf{t}) = u_k(\mathbf{t}) * \left(\delta(\langle \mathbf{t}, \omega_\mathbf{k} \rangle) + \frac{i}{\pi \langle \mathbf{t}, \omega_\mathbf{k} \rangle}\right)\delta(\langle \mathbf{t}, \omega_\mathbf{k}, \perp \rangle),$$
$$\text{(B-3)}$$

where $\omega_\mathbf{k}$ is the frequency vector in the 2D plane. Here, the transform is separable: The analytic signal is calculated line-wise along the direction of $\omega_\mathbf{k}$. The two dimensions are processed independently and show the properties as a 2D Fourier transform.

Appendix C

Seismic spectrum with linear events

We adopt plane-wave assumption to characterize seismic propagation. If there is a linear event, the seismic signal can be expressed as a plane wave:

$$d(t, x) = w\left(t - \frac{x}{c}\right), \qquad \text{(C-1)}$$

where x and t stand for the coordinates of offset axis and time axis, respectively, w is the waveform, such as Ricker wavelet, and c is the wave-propagation velocity.

Applying Fourier transform along t-axis in equation C-1, the f-x spectrum can be obtained

$$D(f, x) = W(f)e^{i\frac{2\pi fx}{c}}, \qquad \text{(C-2)}$$

where f is the frequency and W is the Fourier transform of w.

For the discrete situation, we can assume that the sampling interval in x-axis is Δx, then

$$D_f(m) \equiv D(m\Delta x, f), \qquad m = 1, 2, \ldots, M, \qquad \text{(C-3)}$$

where m is the trace number and M is the total number of the traces.

In addition, there is a constant exponential relationship between two adjacent traces:

$$D_f(m) = D_f(m - 1)e^{i\frac{2\pi f\Delta x}{c}}. \qquad \text{(C-4)}$$

From equation C-4, we know that the frequency slice D_f includes one complex harmonic in the f-x domain. Bekara and van der Baan (2009) conclude that the superposition of p linear events in the t-x domain is equivalent to the superposition of p complex harmonics in the f-x domain.

Thus, based on the IMF definition in Appendix A and the series theory, it is valid to decompose seismic data into IMFs.

References

Bekara, M., and M. van der Baan, 2009, Random and coherent noise attenuation by empirical mode decomposition: Geophysics, **74**, no. 5, V89–V98, doi: 10.1190/1.3157244.

Bülow, T., and G. Sommer, 1999, A novel approach to the 2D analytic signal, *in* Computer Analysis of Images and Patterns, Springer, 25–32.

Cross, T. A., and M. A. Lessenger, 1988, Seismic stratigraphy: Annual Review of Earth and Planetary Sciences, **16**, 319–354, doi: 10.1146/annurev.ea.16.050188.001535.

Dragomiretskiy, K., and D. Zosso, 2014, Variational mode decomposition: IEEE Transactions on Signal Processing, **62**, 531–544, doi: 10.1109/TSP.2013.2288675.

Gautier, D. L., 2003, Carboniferous-Rotliegend total petroleum system description and assessment results summary: U.S. Department of the Interior, U.S. Geological Survey.

Ghazi, S. A., 1992, Cenozoic uplift in the Stord Basin area and its consequences for exploration, *in* L. N. Jense, and F. Riis, eds., Post-Cretaceous uplift and sedimentation along the western Fennoscandia Shield: Norsk Geologisk Tidsskrift 72, 285–290.

Gilles, J., 2013, Empirical wavelet transform: IEEE Transactions on Signal Processing, **61**, 3999–4010, doi: 10.1109/TSP.2013.2265222.

Han, J., and M. Van der Baan, 2013, Empirical mode decomposition for seismic time-frequency analysis: Geophysics, **78**, no. 2, O9–O19, doi: 10.1190/geo2012-0199.1.

Hart, B. S., 2013, Whither seismic stratigraphy?: Interpretation, **1**, no. 1, SA3–SA20, doi: 10.1190/INT-2013-0049.1.

Honorio, B., A. Vidal, and M. Matos, 2016, Progress on empirical-mode decomposition-based techniques and its impacts on seismic-attribute analysis: 86th Annual International Meeting, SEG, Expanded Abstracts, 2118–2122.

Huang, N. E., Z. Shen, S. R. Long, M. C. Wu, H. Shih, Q. Zheng, N.-C. Yen, C. Tung, and H. Liu, 1998, The empirical mode decomposition and the Hilbert spectrum for nonlinear and non-stationary time series analysis: Proceedings of the Royal Society of London: Mathematical, Physical and Engineering Sciences, **454**, 903–995, doi: 10.1098/rspa.1998.0193.

Hunt, D., and M. E. Tucker, 1992, Stranded parasequences and the forced regressive wedgesystems tract: Deposition during base-level fall: Sedimentary Geology, **81**, 1–9, doi: 10.1016/0037-0738(92)90052-S.

Hunt, D., and M. E. Tucker, 1995, Stranded parasequences and the forced regressive wedgesystems tract: Deposition during base-level fall — Reply: Sedimentary Geology, **95**, 147–160, doi: 10.1016/0037-0738(94)00123-C.

Kaplan, S. T., M. D. Sacchi, and T. J. Ulrych, 2009, Sparse coding for data-driven coherent and incoherent noise attenuation: 79th Annual International Meeting, SEG, Expanded Abstracts, 3327–3331.

Li, F. Y., S. Verma, H. Zhou, T. Zhao, and K. J. Marfurt, 2016a, Seismic attenuation attributes with applications on conventional and unconventional reservoirs: Interpretation, **4**, no. 1, SB63–SB77, doi: 10.1190/INT-2015-0105.1.

Li, F. Y., T. Zhao, Y. Zhang, and K. J. Marfurt, 2016b, VMD based sedimentary cycle division for unconventional facies analysis: Unconventional Resources Technology Conference, SEG/AAPG/SPE, 1311–1319, doi: 10.15530/urtec-2016-2455478.

Ligtenberg, H., G. de Bruin, and N. Hemstra, 2006, Sequence stratigraphic interpretation in the wheeler transformed (flattened) seismic domain: 68th Annual International Conference and Exhibition, EAGE, Extended Abstracts, doi: 10.3997/2214-4609.201402337.

Liu, W., S. Cao, and Y. Chen, 2016, Applications of variational mode decomposition in seismic time-frequency analysis: Geophysics, **81**, no. 5, V365–V378, doi: 10.1190/geo2015-0489.1.

Liu, Y., G. Yang, and W. Cao, 2015, The division of sedimentary cycle based on HHT: 85th Annual International Meeting, SEG, Expanded Abstracts, 1902–1906.

Lu, W. K., and F. Y. Li, 2013, Seismic spectral decomposition using deconvolutive short time Fourier transform spectrogram: Geophysics, **78**, no. 2, V43–V51, doi: 10.1190/geo2012-0125.1.

Martins-Neto, M. A., and O. Catuneanu, 2010, Rift sequence stratigraphy: Marine and Petroleum Geology, **27**, 247–253, doi: 10.1016/j.marpetgeo.2009.08.001.

Mitchum, R. M., P. R. Vail, Jr., and S. Thompson III, 1977, Seismic stratigraphy and global changes of sea level: Part 2 — The depositional sequence as a basic unit for stratigraphic analysis, *in* C. E. Payton, ed., Seismic stratigraphy: Applications to hydrocarbon exploration: AAPG Memoir 26, 53–62.

Overeem, I., G. J. Weltje, C. BishopKay, and S. B. Kroonenberg, 2001, The Late Cenozoic Eridanos delta system in the Southern North Sea Basin: A climate signal in sediment supply?: Basin Research, **13**, 293–312, doi: 10.1046/j.1365-2117.2001.00151.x.

Partyka, G., J. Gridley, and J. Lopez, 1999, Interpretational applications of spectral decomposition in reservoir characterization: The Leading Edge, **18**, 353–360, doi: 10.1190/1.1438295.

Patruno, S., G. J. Hampson, and C. A. Jackson, 2015, Quantitative characterisation of deltaic and subaqueous clinoforms: Earth-Science Reviews, **142**, 79–119, doi: 10.1016/j.earscirev.2015.01.004.

Perez, R., and K. J. Marfurt, 2014, Mineralogy-based brittleness prediction from surface seismic data: Application to the Barnett Shale: Interpretation, **2**, no. 4, T255–T271, doi: 10.1190/INT-2013-0161.1.

Plint, A. G., and D. Nummedal, 2000, The falling stage systems tract: Recognition and importance in sequence stratigraphic analysis, *in* D. Hunt, and R. L. Gawthorpe, eds., Sedimentary response to forced regression: Geological Society, London, Special Publications 172, 1–17.

Posamentier, H. W., and G. P. Allen, 1999, Siliciclastic sequence stratigraphy: Concepts and applications: SEPM Concepts in Sedimentology and Paleontology 7.

Rider, M. H., 1999, Geologic interpretation of well logs: Whittles Publishing Services.

Sales, J. K., 1992, Uplift and subsidence of northwestern Europe: Causes and influence on hydrocarbon entrapment, *in* L. N. Jense, and F. Riis, eds., Post-Cretaceous uplift and sedimentation along the western Fennoscandia Shield: Norsk Geologisk Tidsskrift 72, 253–258.

Sinha, S., P. S. Routh, P. D. Anno, and J. P. Castagna, 2005, Spectral decomposition of seismic data with continuous-wavelet transform: Geophysics, **70**, no. 6, P19–P25, doi: 10.1190/1.2127113.

Tary, J. B., R. H. Herrera, J. Han, and M. van der Baan, 2014, Spectral estimation — What is new? What is next?: Reviews of Geophysics, **52**, 723–749, doi: 10.1002/2014RG000461.

Vail, P. R., 1987, Seismic stratigraphy interpretation procedure, *in* A. W. Bally, ed., Atlas of seismic stratigraphy: AAPG Studies in Geology 27, 1–10.

Vail, P. R., R. M. Mitchum, Jr., and S. Thompson III, 1977, Seismic stratigraphy and global changes of sea level: Part 3 — Relative changes of sea level from coastal onlap, *in* C. E Payton, ed., Seismic stratigraphy — Applications to hydrocarbon exploration: AAPG Memoir 26, 63–81.

Wang, Y., 2007, Seismic time-frequency spectral decomposition by matching pursuit: Geophysics, **72**, no. 1, V13–V20, doi: 10.1190/1.2387109.

Wang, X., B. Zhang, F.Y. Li, J. Qi, and B. Bai, 2016, Seismic time-frequency decomposition by using a hybrid basis-matching pursuit technique: Interpretation, **4**, no. 2, T239–T248, doi: 10.1190/INT-2015-0208.1.

Zeng, H., 2013, Frequency-dependent seismic-stratigraphic and facies interpretation: AAPG Bulletin, **97**, 201–221, doi: 10.1306/06011212029.

Zhao, T., F. Y. Li, and K. J. Marfurt, 2017, Constraining self-organizing map facies analysis with stratigraphy: An approach to increase the credibility in automatic seismic facies classification: Interpretation, **5**, no. 2, T163–T171, doi: 10.1190/INT-2016-0132.1.

Fangyu Li received a B.E. (2009) and an M.S. (2013) in electrical engineering from Beihang University and Tsinghua University, respectively. He is a Ph.D. candidate in geophysics at the University of Oklahoma. His current research interests include subsurface imaging, signal processing, and quantitative seismic interpretation.

Bo Zhang received a B.S. (2002) from the China University of Petroleum (Huadong) and an M.S. (2006) in geophysics from the Institute of Geology and Geophysics, Chinese Academy of Sciences. In 2009, he joined an industry-supported consortium (AASPI) at the University of Oklahoma as a Ph.D. student in geophysics. In 2014, he joined the Michigan Technological University as a visiting assistant professor. In 2015, he joined the University of Alabama as an assistant professor. His current research interests include broadband seismic data processing, development and calibration of new seismic attributes, pattern recognition of geologic features on 3D seismic data, and shale resource play characterization.

Rui Zhai received a Ph.D. (2013) in geology from the China University of Petroleum, Beijing. He is now a post-doctoral researcher at the University of Oklahoma. His current research interests include reservoir characterization, sequence stratigraphy, seismic geomorphology, and seismic attributes analysis.
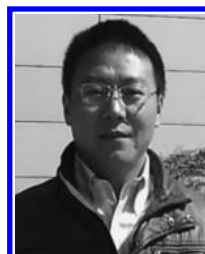
Huailai Zhou received a Ph.D. (2009) in earth exploration and information techniques from the Chengdu University of Technology. He completed his postdoctoral research at the Institute of Sedimentary Geology at the Chengdu University of Technology from 2010 to 2012. He worked as a postdoctoral research faculty member at AASPI in the University of Oklahoma from October 2013 to October 2014. He currently works in the Chengdu University of Technology as a professor, and his research work is mainly focused on seismic data processing methods, seismic modeling and imaging, techniques for improving seismic resolution, seismic attributes analysis, and inversion methods.

Kurt J. Marfurt received a Ph.D. (1978) in applied geophysics from Columbia University's Henry Krumb School of Mines in New York where he also taught as an assistant professor for four years. He joined the University of Oklahoma in 2007, where he serves as the Frank and Henrietta Schultz Professor of Geophysics within the ConocoPhillips School of Geology and Geophysics. His recent work focuses on applying coherence, spectral decomposition, structure-oriented filtering, and volumetric curvature to mapping fractures and karst with a particular focus on resource plays. He worked for 18 years in a wide range of research projects at Amoco's Tulsa Research Center, after which he joined the University of Houston for eight years as a professor of geophysics and the director of the Allied Geophysics Lab. In addition to teaching and research duties at the University of Oklahoma, he also leads short courses on attributes for SEG and AAPG. His primary research interests include development and calibration of new seismic attributes to aid in seismic processing, seismic interpretation, and reservoir characterization.